New Insights into the Mechanism of Permeation through Large Channels

Alexander G. Komarov,*‡ Defeng Deng,† William J. Craigen,† and Marco Colombini*
*Department of Biology, University of Maryland, College Park, Maryland 20742; †Departments of Molecular and Human Genetics and Pediatrics, Baylor College of Medicine, Houston, Texas 77030; and ‡St. Petersburg Nuclear Physics Institute, Gatchina, Russia, 188350

ABSTRACT The mitochondrial channel, VDAC, regulates metabolite flux across the outer membrane. The open conformation has a higher conductance and anionic selectivity, whereas closed states prefer cations and exclude metabolites. In this study five mutations were introduced into mouse VDAC2 to neutralize the voltage sensor. Inserted into planar membranes, mutant channels lack voltage gating, have a lower conductance, demonstrate cationic selectivity, and, surprisingly, are still permeable to ATP. The estimated ATP flux through the mutant is comparable to that for wild-type VDAC2. The outer membranes of mitochondria containing the mutant are permeable to NADH and ADP/ATP. Both experiments support the counterintuitive conclusion that converting a channel from an anionic to a cationic preference does not substantially influence the flux of negatively charged metabolites. This finding supports our previous proposal that ATP translocation through VDAC is facilitated by a set of specific interactions between ATP and the channel wall.

INTRODUCTION

VDAC is known as the major pathway for metabolite flux across the mitochondrial outer membrane (MOM) (1–5). This 30–32 kDa protein forms large channels with a molecular weight cutoff of up to 5000 for nonelectrolytes in the fully open state (6). VDAC has a single open and multiple low-conducting closed states. The diameter of the pore is ~3 nm in the open and 1.8 nm in the closed state based on nonelectrolyte flux and electron microscopic observations of negatively stained two-dimensional crystals (3,7,8). One proposed secondary structure model includes one α-helix and 13 β-strands (9). These 14 elements form a barrel-like transmembrane structure that is tilted at a 45° angle (10).

VDAC from different eukaryotic species share highly conserved electrophysiological properties in vitro (11), including single channel conductance, voltage gating, and ionic selectivity. The open state is characterized by higher conductance (~4 nS in 1 M KCl) and weak anionic selectivity (2:1 in favor of Cl^- over K^+ in a 10-fold KCl gradient). Closed states of VDAC have lower conductance (~50–60% reduction compared to the open state) and cationic selectivity. Transition between the open and closed states is voltage dependent and is the result of the motion of the positively charged voltage sensor (12). At low voltages (<30 mV) this mobile domain forms part of the channel wall, which contributes to the anionic selectivity of the open state. At high voltages the voltage sensor moves out of the lumen of the channel causing channel closure and a switch to cationic selectivity. The voltage dependence has a symmetrical character referring to the sign of the applied voltage (1,13).

Whereas VDAC demonstrates only slight ionic preference in the presence of small ions, the permeability of the open and closed states to metabolites or large anions is dramatically different. Direct measurements of ATP flux have determined that ATP can penetrate through VDAC in the open state, however, it becomes virtually impermeant upon closure of the channel (14). Although the effective diameter of the ATP molecule is only 0.96 nm (calculated from the diffusion coefficient from Rostovtseva et al. (15)), this metabolite cannot pass through the closed state (1.8 nm in diameter). Simple electrostatic repulsion from the channel wall is thought to account for this impermeability.

In previous work we found that the open state of VDAC demonstrates another type of selectivity (15–17). The penetration of large negatively charged molecules through VDAC was monitored by measuring the interference of those substrates to the flow of small ions. This interference can result in two observables: an increase in the current noise and a reduction of the single channel conductance. The current noise increases because as the larger ion moves in and out of the channel it alters the current flow through the channel causing current fluctuations, i.e., current noise. The same phenomenon should be responsible for the reduced time-averaged conductance. Among nucleotides (NADPH, NADH, NAD, ATP, ADP, AMP, UTP) the ability to reduce the single channel conductance was very similar, however, the ability to generate current noise exhibited a strong dependence on the nucleotide base. These observations led us to propose the existence of a nucleotide-binding site within the channel lumen that recognizes purine-containing nucleotides. The reduction in conductance was proposed to be the result of the channel-penetrating ions and this contributed very little to the current noise. The binding of the nucleotide to the site altered the selectivity of the channel resulting in large current changes and thus large current noise.

The same experimental approach revealed the ability of VDAC to differentiate between metabolites and synthetic molecules. Synthetic anions such as tetraglutamate and 1-hydropyrene-3,6,8-trisulfate, which have an effective size

Submitted July 5, 2005, and accepted for publication September 8, 2005.
Address reprint requests to Marco Colombini, E-mail: colombin@umd.edu.

0006-3495/05/12/3950/10 $2.00
doi: 10.1529/biophysj.105.070037

and charge comparable to ATP, did not interfere with the flux of small ions, indicating that these ions could not permeate through VDAC. Noise analysis also did not provide any evidence for the penetration of these molecules into the channel. This set of experiments showed that VDAC has a special type of selectivity for large anions. This selectivity is based on the shape of the molecule and charge distribution rather than just charge and effective size.

In this work we demonstrate that the permeability of VDAC to metabolites is defined by a specific interaction between metabolites and the channel wall rather than by the overall charge of the channel lumen.

MATERIALS AND METHODS

Preparation of yeast cells

M3 (*MATα lys2 his4 trp1 ade2 leu2 ura3*) is the parental wild-type strain (with respect to *POR1*). M22-2 (Δ*por1*) lacks *POR1* due to the insertion of the yeast *LEU2* gene at the *POR1* locus (18). To generate a wild-type mouse VDAC2 (mVDAC2) yeast shuttle vector, oligonucleotide-directed mutagenesis was used to create a *Nco*I site at the start codon and a *Nsi*I site within the 3′ untranslated region. This allowed for the complete open reading frame of the mVDAC2 cDNA to precisely replace the yeast VDAC1 gene previously subcloned into a single-copy yeast shuttle vector (pSEYC58), as described (19), placing expression of the engineered gene under the control on the endogenous transcriptional control elements. For site-directed mutagenesis of individual amino acids, oligonucleotide primers were designed according to the desired amino acid substitution. The sequences of the oligonucleotides are listed in Table 1. PCR-based mutagenesis was performed using a commercial kit following the manufacturer's protocol (QuickChange XL site-directed mutagenesis, Stratagene, La Jolla, CA). Each substitution was created sequentially and confirmed by DNA sequencing. The relevant mutant mVDAC2 (K19E-K31E-K60E-K95E-D227K) was introduced into M22-2 using a shuttle vector, as previously described (19).

To facilitate cell growth and harvesting, stock cultures were prepared (following Lee et al. (4)) by inoculating a single colony into 50 ml of medium consisting of 335 mg of Difco yeast nitrogen base without amino acids (No. 291940, Becton, Dickinson and Company, Sparks, MD), 50 mg of KH_2PO_4, 38.5 mg of CSM-URA (No. 4511-222, complete supplement mixture minus Uracil; Q-BIOgene, Carlsbad, CA), and 1 ml of 85% lactic acid. The medium was adjusted to pH 5.5 by adding of solid KOH. Autoclaving time and temperature were reduced (110°C, 15 min) to minimize pH drop and achieve good growth characteristics. When the cells reached an optical density of between 0.7 and 0.9 O.D. (at 600 nm) they were stored at 4°C for later use. For mitochondrial isolation, 9 ml of yeast stock solution were inoculated into each of two flasks containing 1 liter of the same medium and grown with orbital shaking at 30°C. A final O.D. between 0.7 and 0.9 gave ~4–5 g of cells.

TABLE 1 Oligonucleotides used to generate the amino acid substitutions

Primer name	Sequence
K19E For	cagagacattttcaac***gaa***ggatttggctttgg
K19E Rev	ccaaagccaaatcc***ttc***gttgaaaatgtctctg
K31E For	gctggatgtg***gaa***acgaagtcatgcagcggtgtgg
K31E Rev	caccgctgcatgacttcgt***ttc***cacatccagc
K60E For	gcgggaccttggagacc***gaa***tacaaatggtgtg
K60E Rev	cacaccatttgta***ttc***ggtctccaaggtcccgctaa
K95E For	tgtcaaggtttg***gaa***ctgacttttgacaccacc
K95E Rev	ggtggtgtcaaaagtcag***ttc***caaaccttgac
D99K For	actgacttt***aaa***accacctttcaccgaacacagg
D99K Rev	cctgtgttcggtgaaaaggtggt***ttt***aaaagtcag
D127K For	cctcggctgt***aaa***gttgactttgattttgc
D127K Rev	ccagcaaaatcaaagtcaac***ttt***acagccgagg
D227K For	ctaaataccagttg***aaa***cctactgcttctatctctgc
D227K Rev	gcagagatagaagcagtagg***ttt***caactggtatttagc

Isolation of intact yeast mitochondria

Mitochondria were isolated from *Saccharomyces cerevisiae* essentially as published (20), but modified as previously described (4) to obtain highly intact mitochondria. The final mitochondrial pellet was suspended in ~1 ml of medium containing 0.6 M mannitol, 10 mM Tris•Cl, 0.6% PVP, 0.1 mM EGTA, and 0.1% BSA, pH 7.2. Mitochondrial protein was measured by the method of Clarke (21). The protein concentration in mitochondrial suspension was 10–15 mg/ml.

Assessing MOM integrity

The integrity of the MOM of purified mitochondria was determined based on the rate of cytochrome-*c*-dependent oxygen consumption (22). Exogenously added cytochrome *c* should reach the mitochondrial inner membrane to be oxidized by cytochrome *c* oxidase. In this case, the outer membrane serves as a barrier for the reaction. The rates of oxygen consumption for intact (υ_{intact}) and osmotically shocked mitochondria ($\upsilon_{disrupted}$) were compared and the percentage of intact mitochondrial was calculated as follows:

$$\%\,\text{intact} = (1 - \upsilon_{intact}/\upsilon_{disrupted}) \times 100.$$

Osmotic shock was applied by mixing of 40 μl of mitochondrial suspension with 1.5 ml of water, incubating for 3 min, and further addition of the double concentrated respiration buffer (1.3 M sucrose, 20 mM HEPES, 20 mM KH_2PO_4, 10 mM KCl, 10 mM $MgCl_2$, pH 7.2) to restore the initial osmotic pressure.

Oxygen consumption was measured by using a Clark oxygen electrode. An aliquot of ascorbate (50 μl of 0.48 M) was added to the 3-ml volume of R-medium (0.65 M sucrose, 10 mM HEPES, 10 mM KH_2PO_4, 5 mM KCl, 5 mM $MgCl_2$, pH 7.2) containing either intact or disrupted mitochondria to maintain the cytochrome *c* in the reduced form. The addition of 180 μg of cytochrome *c* was used to induce oxygen consumption. Finally, an aliquot of KCN (0.2 mM final) was used to block cytochrome *c* oxidase and determine the level of KCN-independent respiration.

Integrity of mitochondria varied from 78 to 86%.

Measurements of outer membrane permeability

Permeability to NADH

To determine MOM permeability we used the method previously reported (4) for yeast mitochondria. NADH added to isolated yeast mitochondria is oxidized primarily by an NADH dehydrogenase located on the outer surface of the inner membrane (23). The rate of NADH oxidation can be limited by the flux of NADH through the MOM.

The permeability of the MOM to NADH was determined by assuming that the rate of NADH oxidation for intact mitochondria is identical to the net flux of NADH through the membrane and dividing this rate by the concentration difference of NADH across the membrane. The medium NADH concentration was monitored directly by measuring the absorbance at 340 nm. The intermembrane space NADH concentration was estimated from the oxidation rate of shocked mitochondria. We assumed that: i), in the disrupted mitochondria the NADH concentration in the intermembrane space is the same as in the medium; and ii), the same local NADH

concentration in the vicinity of the dehydrogenase results in the same oxidation rate. Thus, the NADH concentration in the intermembrane space is the same as the concentration needed to achieve the same oxidation rate in disrupted mitochondria. At low NADH concentrations the calculated permeability values are not meaningful because the concentration differences are insignificant when compared to the noise.

Samples of intact mitochondria were prepared by 10-fold dilution of the mitochondrial suspension (0.7–3.0 mg/ml of total protein) with R-medium. Disrupted mitochondria were obtained by using a mild osmotic shock as previously described (4). One volume of mitochondrial suspension was mixed with 2 vol of distilled water and incubated in ice for 10 min. Then, 5 vol of R-medium and 2 vol of double concentrated R-medium were added to restore the initial osmotic pressure. The uncoupler, FCCP (3 μM final concentration), was added to both intact and shocked mitochondrial samples to ensure that the membrane potential would not inhibit the rate of NADH oxidation. An aliquot of NADH (30 μM final concentration) was added to start the reaction.

Permeability to ADP/ATP

To estimate the permeability of the intact MOM to ADP/ATP we used a method similar to that described for NADH. The flux of ADP/ATP across MOM was determined by comparing the activity of adenylate kinase in suspensions of intact and osmotically shocked mitochondria. The intermembrane space enzyme adenylate kinase was assayed by a standard method (24), using a coupled enzyme system (hexokinase and glucose-6-phosphate dehydrogenase) and detecting the rate of $NADP^+$ reduction.

Like NADH, access of externally added ADP to the intermembrane space may be limited by the permeability of the MOM. The consumption of ADP can be indirectly determined by the rate of the reduction of externally added $NADP^+$. Two molecules of ADP enter the intermembrane space through the outer membrane and are transformed by adenylate kinase to ATP and AMP. ATP must cross the outer membrane to be consumed by the coupled enzyme system (hexokinase and glucose-6-phosphate dehydrogenase) and glucose to produce NADPH (monitored at 340 nm). ATP cannot move to the matrix because the adenine nucleotide translocator was blocked by atractyloside (20 μg/ml final concentration). Oxidation of NADPH was blocked by the use of CN^- (0.2 mM).

A similar approach to that used for NADH was used to calculate the permeability of the MOM to ADP/ATP. However, the situation is more complex because adenylate kinase is located in the intermembrane space and the added enzymes are in the medium. Thus, at steady state the overall rate of NADPH production must be equal to net efflux of ATP from the mitochondrion to the medium and equal to one half the net flux of ADP into the mitochondrion (reflecting the stoichiometry of adenylate kinase). The [ADP] is known because it must be the initial concentration minus the [NADPH] that is measured continuously. The [ADP] in the intermembrane space required to maintain the correct ADP flux is not known. The medium [ATP] should be very low because of the action of hexokinase. Again, the [ATP] in the intermembrane space needed to achieve the correct flux of ATP is not known. However, the rate of adenylate kinase activity, which must be the same as the rate of NADPH production, will be reduced by the presence of ATP in the intermembrane space, as dictated by the known kinetics of the enzyme. We determined the [ATP] in the intermembrane space by measuring the reduction of the rate of NADPH production when the MOM is intact. We assumed that when the MOM is disrupted hexokinase maintains the [ATP] near zero.

Kinetic studies of yeast adenylate kinase (25) have shown that the reaction is limited by the rate of conversion of the enzyme from E-ADP_2 to E-AMP-ATP. Thus, we were able to assume that the binding steps in the adenylate kinase reaction were at equilibrium. We established a spreadsheet to model the adenylate kinase reaction and constrained it using the published V_{max} and K_m values for the forward and reverse reactions ($K_{ADP} = 2.7 \times 10^{-4}$ M, $K_{AMP} = 5.8 \times 10^{-5}$ M, and $K_{ATP} = 5.4 \times 10^{-5}$ M; $V_{reverse} = 2.14 \times V_{forward}$). We further assumed independence of the binding constants of all substrates. The model yielded the following binding constants: $k_{ADP} = 6.0 \times 10^3$ M, $k_{AMP} = 4.5 \times 10^4$ M, and $k_{ATP} = 4.5 \times 10^4$ M. The model then was used to determine the [ATP] that would cause the observed reduction in the adenylate kinase reaction rate.

Samples of intact mitochondria were prepared by 40-fold dilution of the mitochondrial suspension (10–14 mg/ml of total protein) with A-medium (0.6 M sucrose, 50 mM Tris•Cl, 5 mM $MgSO_4$, 10 mM glucose, 0.2 mM $NADP^+$, 20 μg/ml atractylosides, 0.2 mM KCN, pH 7.5). Disrupted mitochondria were obtained by using a mild osmotic shock. One volume of mitochondrial suspension was mixed with 9 vol of distilled water and incubated in ice for 5 min. Ten volumes of double concentrated A-medium and 20 vol of A-medium were then added to restore the initial osmotic pressure. An aliquot containing ADP (250 μM final concentration), hexokinase, and glucose-6-phosphate dehydrogenase (10 units each) was added to start the reaction.

Purification of the mVDAC2 mutant

The mVDAC2 mutant was isolated from mitochondrial membranes and purified according to standard methods (26,27). The final mitochondrial suspension was hypotonically shocked in 1 mM KCl, 1 mM HEPES, pH 7.5, to disrupt the mitochondrial membranes and release soluble proteins. The membranes were sedimented at 24,000 $\times$ *g* for 20 min. The pellet was resuspended in a buffer consisting of 15% DMSO, 2.5% Triton X-100, 50 mM KCl, 10 mM Tris•Cl, 1 mM EDTA, pH 7.0, and sedimented in a microcentrifuge at 14,000 rpm for 30 min. The supernatant was passed through a column containing a 1:1 mixture of hydroxyapatite/celite that, at low ionic strength, binds most proteins but allows VDAC to flow through. Samples of mutant VDAC were stored at -85°C for the future use.

Channel conductance measurements

Planar membranes were formed from monolayers made from a solution containing 0.5% of diphytanoylphosphatidylcholine, 0.5% of asolectin-soybean phospholipid (both from Avanti Polar Lipids, Alabaster, AL) and 0.1% cholesterol (Sigma, St. Louis, MO) in hexane. The two monolayers form a bilayer membrane across a 70–90-μm diameter aperture in a 15-μm-thick Teflon partition that separates two chambers (modified Montal and Mueller technique (28)). The total capacitance is typically 70–80 pF and the film capacitance is 30–35 pF. Aqueous solutions of 1.0 M or 0.10 M NaCl or KCl, 1 mM $MgCl_2$, 1 mM $CaCl_2$ were buffered with 5 mM HEPES at pH 7.0. All measurements were made at room temperature.

Channel insertion was achieved by adding of 0.2–2.0 μl of a 2.5% Triton X-100 solution of purified mVDAC2 mutant protein to the 2.5-ml aqueous phase in the ''*cis*'' compartment while stirring.

The membrane potential was maintained using Ag/AgCl electrodes with 3.0 M KCl, 15% agarose bridges assembled within standard 200 μl pipette tips (29). The potential is defined as positive when it is greater on the side of protein addition (*cis*). The current was amplified by an Axopatch 200B amplifier (Axon Instruments, Foster City, CA) set to the voltage clamp mode.

The change in the conductance of mVDAC2 mutant protein upon addition of ATP was studied as previously described (15). After single channel parameters were recorded, membrane-bathing solutions in both compartments were replaced by the same solutions containing ATP. The fresh, denser solution was added to the bottom of the chamber and the old solution was removed from the top. This procedure allows for the detection of the effect of nucleotide on the same channel.

Reversal potential measurements

The reversal or zero-current potential was measured to assess the selectivity in single or multichannel membranes. The reversal potential of an ideally cation-selective membrane was found by measuring the reversal potential of a synthetic ion exchange membrane under identical conditions. Because the same electrodes and the same solutions were used to record reversal

potentials for ideally cation-selective membranes and the VDAC-doped membranes, electrode asymmetries and liquid junction potentials influence both sets of measurements identically.

We used a 10-fold gradient of KCl, 1.0 M *cis* and 0.10 M *trans*, plus HEPES as above, and a fourfold gradient of disodium ATP salt (SigmaUltra, Sigma-Aldrich, St. Louis, MO) adjusted to pH 7.0 with NaOH. An aliquot of a solution containing the mVDAC2 mutant protein was added to the side with the higher concentration. Results are expressed as mean ± SD.

Quantifying purified mVDAC2 protein

To compare the levels of expression of wild-type and mutant mVDAC2 we used standard SDS-page electrophoresis procedure (30). Both wild-type and mutant proteins were purified from the equal amounts of mitochondria (measured by total protein concentration). After the addition of concentrated sample buffer, samples were separated on a 10% acrylamide gel supplemented with 4 M urea and the bands stained with GelCode blue stain (Pierce, Rockford, IL). Molecular weight standards were purchased from Invitrogen (BenchMark Protein Ladder, No. 10747-012, Carlsbad, CA). Densitometry was performed using the AlphaImager 2000 documents and analysis system and AlphaImager 3.2 software (both from Alpha Innotech, San Leandro, CA).

RESULTS

The initial purpose of this study was to obtain a voltage-independent mutant form of the mVDAC2 isoform that is constitutively impermeable to anionic metabolites. Five amino acid substitutions were engineered into mVDAC2: K19E, K31E, K60E, K95E, D227K (Fig. 1; the folding pattern was generated by analogy with *Neurospora crassa* VDAC (9)). The rationale for choosing these residues is as follows. The first three mutations were designed to neutralize the voltage sensor that is responsible for VDAC's voltage gating. This should keep the channel in the open conformation but reduce the net positive charge in the channel responsible for favoring the flux of anions. This mutant molecule was expressed in a yeast strain lacking the endogenous VDAC1 gene (Δ*por1*). The Δ*por1* strain is characterized by a temperature-dependent growth-restrictive phenotype when cultured on a nonfermentable carbon source such as glycerol; cells are able to grow at 30°C, but not 37°C (18). It has previously been observed that mouse VDACs expressed in the Δ*por1* background rescue this conditional phenotype, allowing for growth on glycerol at 37°C (19,31). However, this mutated mVDAC2, when expressed in the Δ*por1* strain, failed to rescue the conditionally growth-restrictive phenotype at 37°C, although it demonstrated normal growth at 30°C (results not shown).

The properties of the mutant mVDAC2 protein resemble those of the closed state of VDAC

After isolation from yeast cells, the mouse VDAC2 mutant was tested for its ability to form channels in planar phospholipid membranes. Upon insertion, the mutant demonstrated a lower conductance (2.1 ± 0.1 ($n = 7$) nS in 1 M KCl) than wild-type mVDAC2 (3.8 nS; Xu et al. (5)) and was able to gate in that the channel could close to a very low conducting state but this closure did not depend on voltage (Fig. 2 *A*). Lack of voltage-dependent gating was clearly demonstrated by applying triangular voltage waves (Fig. 2 *B*). The rate of change of voltage with time used is very similar to that typically used to examine the voltage dependence of wild-type VDAC. The current-voltage relation showed rectification, which would be expected if the charges introduced were not arranged symmetrically along the length of the channel. In addition, the mutant channel showed selectivity for small cations (K^+) over small anions (Cl^-). The reversal potential of -24.3 ± 1.4 ($n = 7$) mV (on the high salt side) for a 10-fold salt gradient yields a permeability ratio, based on Goldman-Hodgkin-Katz theory, of 4.1:1 in favor of K^+. Also the mutant occasionally demonstrated fast gating at low voltage (Fig. 2 *C*). Most of these properties resemble the closed state of wild-type VDAC.

The mutant mVDAC2 protein is permeable to ATP

Fig. 3 shows a time course of the perfusion of the *cis* side with an ATP solution (81 mM final), followed by a drop in the channel conductance. The perfusion increased the conductivity of the aqueous bulk electrolyte by 5%. This change in the conductivity was best compensated for in experiments where ATP was added symmetrically. In these experiments the channel conductance dropped by ~20% relative to the medium conductivity (from 2.1 to 1.7 nS). This indicates that ATP interferes with the flow of small ions and thus enters the channel lumen. Interestingly, the addition of the same concentration of HPTS (1-hydroxypyrene-3,6,8-trisulfate), which is a synthetic molecule with similar size and charge as ATP that does not permeate through VDAC (17), did not have any effect on the single channel conductance (data not shown).

Measurements of the channel selectivity in the presence of a sodium ATP salt gradient (200 vs. 50 mM) supported our conclusion that the mutant is permeable to ATP. Membranes containing the mutant channel had a reversal potential of -20 ± 1 ($n = 4$) mV (Fig. 4), but control experiments with a cation-selective membrane yielded a reversal potential of -26 ± 1 ($n = 4$) mV. Combining these values with the current at zero voltage, we estimated the flux of ATP through the mutant channel as 3.3×10^6 ions/s (see Appendix), and this is comparable with the value for the wild-type VDAC (32).

Expression of mutant mVDAC2 permeabilizes the MOM to ATP and NADH

Fig. 5 illustrates the rate of NADH oxidation by intact and osmotically shocked mitochondria when either mouse VDAC2 (*A*), the mutant (*B*), or no VDAC (ΔPOR1) (*C*) were expressed. In all cases the rate of NADH oxidation was higher when the outer membrane was damaged (Fig.5, *insets*),

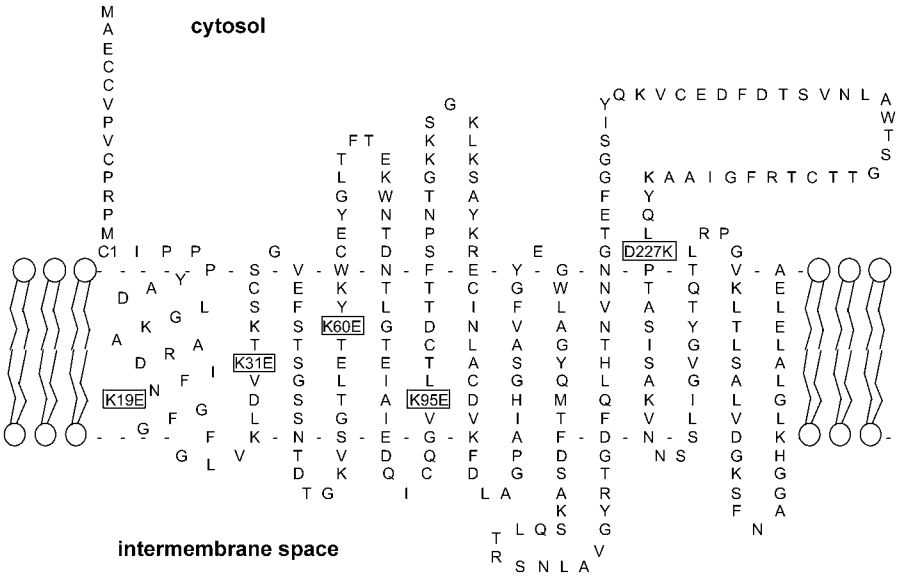

FIGURE 1 The folding pattern for mouse VDAC2 isoform. Boxes indicate points and type of mutation.

thus removing the barrier to flow. However, the difference in the rate of NADH oxidation varies, reflecting differences in permeability. Mitochondria containing wild-type mVDAC2 showed the smallest difference, indicating the highest permeability to NADH. The calculated permeability of mitochondria containing mutant mVDAC2 is almost 10-fold smaller than for those containing wild-type mVDAC2, but is still larger than the permeability of mitochondria lacking VDAC (Fig. 6). This relationship may reflect different expression levels for the mutant and wild-type mVDAC2.

To address this possibility we performed electrophoresis analysis after loading equal amounts of each protein. For correct normalization both the mutant and wild-type mVDAC2 proteins were purified from mitochondrial preparations containing an equal amount of total protein. Fig. 7 demonstrates that the expression level of the mutant was almost half that of the wild-type mVDAC2. Densitometric quantitation of the bands and comparison with the known amount of protein standards revealed 2.3 μg of the mutant and 4.3 μg of wild-type mVDAC2 per band. Thus, yeast mitochondria with a total protein amount of 15 mg contain $\sim$0.09 μg of the mutant or 0.17 μg of wild-type mVDAC2. Hence, after compensating for the protein content, the permeability of the mutant mVDAC2 to NADH is only five times smaller than that for wild-type mVDAC2.

The permeability to ADP/ATP was determined by measuring adenylate kinase activity. When wild-type mVDAC2 was expressed the difference in adenylate kinase activity between intact and shocked mitochondria was small (Fig. 8 *A*). This is consistent with almost free diffusion of ADP/ATP across the MOM of intact mitochondria. The difference was larger in the presence of the mutant mVDAC2 (Fig. 8 *B*), and much larger when no VDAC was expressed (Fig.8 *C*). High initial rates were due to an estimated 1% contamination of ATP in the ADP powder used for the preparation of solutions (from control experiments with no added adenylate kinase).

Fig. 9 summarizes permeability values for all three samples. The permeability of the mutant mVDAC2 protein to ADP/ATP was half the permeability of wild-type mVDAC2. This could be explained simply by the difference in protein expression, as discussed above. Thus, we can conclude that the mutations reduced only the permeability to NADH whereas the permeability to ADP/ATP essentially does not change. This is in agreement with our estimation of ATP flux through the mutant mVDAC2 protein based upon planar membrane experiments.

DISCUSSION

Large channels are traditionally considered as ''molecular sieves'' that differentiate between molecules based only on their size and charge. Typically they exhibit weak ionic selectivity that is presumed to be the result of general electrostatic interactions between a charged permeant and the channel wall. However, there are examples of high levels of selectivity in channels with a large pore diameter that is similar to the selectivity displayed by Na^+, K^+, or Cl^- channels. These examples include maltoporin (also referred to as LamB), OmpF, and VDAC. Maltoporin, which is involved in the transport of maltose (33), was shown to favor maltooligosaccharide flux over the flux of other oligosaccharides (34). This selectivity was found to be the result of a specific interaction between maltodextrins and the channel wall (35). OmpF exhibits preferential flux for certain antibiotics like ampicillin and several other penicillins used to kill *Escherichia coli*. However, it is not effective at transporting other ''nonspecific'' antibiotics (36). The specificity

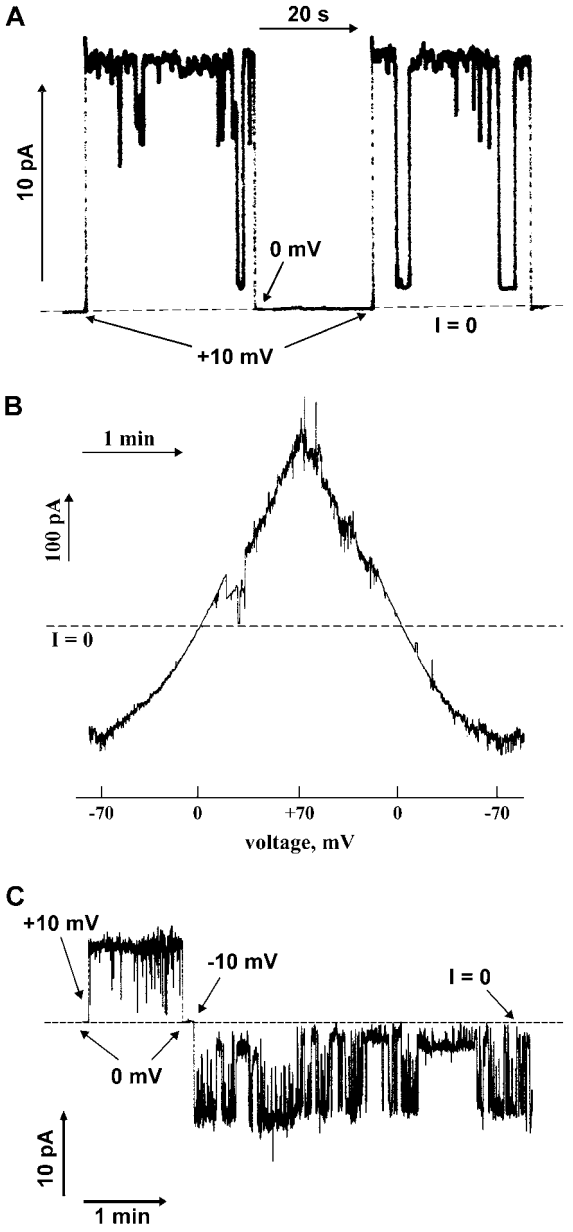

FIGURE 2 Changes in ionic current through a planar membrane in the presence of mouse VDAC2 mutant. (*A*) Insertion and gating of a single channel in 1.0 M NaCl. (*B*) Current through a few channels as a function of voltage in 1.0 M KCl (voltage was applied in the form of a triangular wave (3 mHz)). (*C*) Fast gating at low voltage in 1.0 M NaCl.

shown by VDAC for the permeation of large anions, as described in the introduction, provides an example of large, highly selective channels in eukaryotes.

The affinity of VDAC for metabolites might be closely related to its function as a regulator of metabolite flux between mitochondrial spaces and the cytosol. The existence of a specific binding site may play a crucial role in providing sufficient nucleotide translocation under conditions of high energy demand, when the rate of flux through VDAC

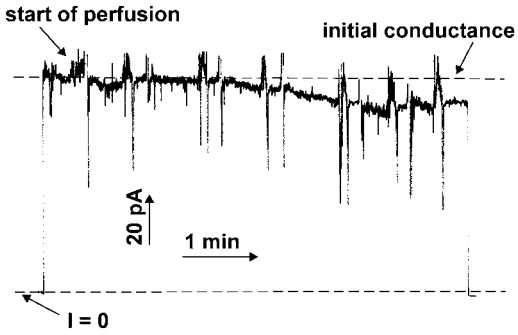

FIGURE 3 ATP addition (81 mM final) to one side of the membrane reduced the current flow through four channels (in 1.0 M KCl). The noise was caused by six steps of manual perfusion. The imposed asymmetry caused a small shift of zero current.

becomes limiting (37,38) and may have an impact on cell survival. In this case, the binding site might accelerate the flow of crucial metabolites, particularly adenine nucleotides. This correlation of binding site specificity with physiological advantage is based on the presumption that it arises from evolutionary selection pressure. Clearly binding can exist with nonphysiologically relevant molecules such as polyethylene glycol binding to α-hemolysin (39). However, our finding, combined with our previously published results argue strongly for a specific site.

Physically, the role of the binding site on the channel wall can be understood by the model of Berezhkovskii and Bezrukov (40). According to this model the binding site provides the potential well in which an optimal depth increases the probability of substrate translocation through the channel, while at the same time does not lead to significant occlusion of the pore. In other words, a capturing of the molecule entering the lumen of the channel by the potential well (i.e., binding site) allows it to ''forget'' which entrance it came

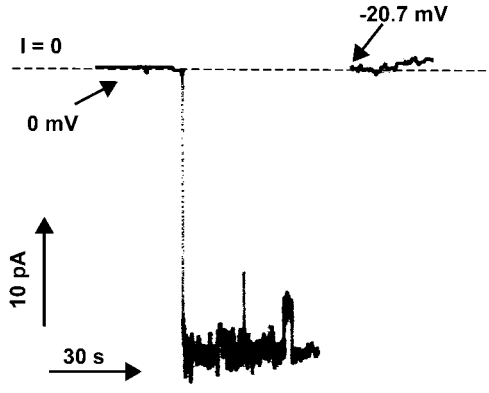

FIGURE 4 In the presence of a fourfold gradient of sodium ATP (200 vs. 50 mM) mVDAC2 mutant demonstrated cationic selectivity. The voltage was applied to the high salt side. The initial sudden change in conductance is due to the insertion of a single channel.

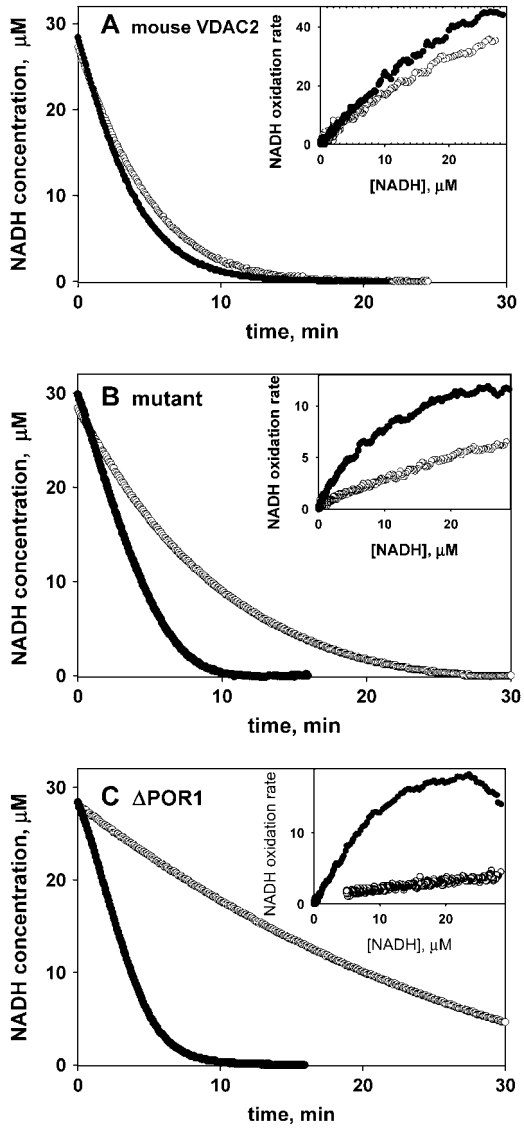

FIGURE 5 NADH oxidation by mitochondria isolated from yeast (lacking the yeast VDAC1 gene) expressing mouse VDAC2 (*A*), the mutant (*B*), or no VDAC (*C*). Oxidation by intact mitochondria (○); oxidation by osmotically shocked mitochondria (●). The oxidation rate in nmol/min/mg protein (*inset*) was calculated as described in Methods. Concentrations of mitochondrial protein were: 110 μg/ml (*A*), 70 μg/ml (*B*), and 300 μg/ml (*C*).

from and hence the probability of successful translocation is increased.

Results of the current work support the existence of a binding site on VDAC for ATP and other nucleotides. We were able to generate a mouse VDAC2 mutant for which the conductance properties resemble the closed state of the wild-type channel. Introduced mutations inactivated the voltage sensor (which resulted in the lack of the voltage-dependent gating) and changed the net charge of the channel lumen, i.e., the selectivity of the channel became cationic without regard for the applied voltage. In this situation we expected that the mutant channel would be permanently closed to metabolites,

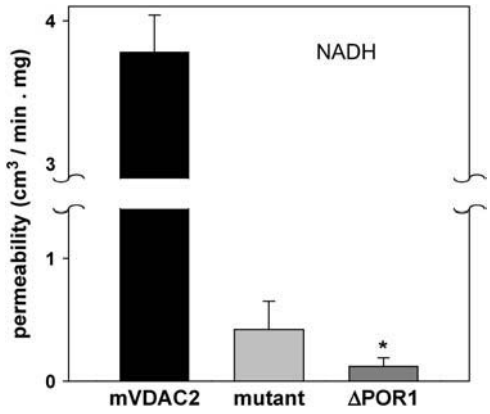

FIGURE 6 A comparison of the average permeability (per milligram protein) of the MOM to NADH in the presence of mouse VDAC2, the mutant, or in the absence of VDAC (ΔPOR1). The average and the standard deviation were calculated based on the results for different batches of mitochondria (three for mouse VDAC2, five for the mutant, and two for ΔPOR1. The average permeability for each batch was obtained from three independent measurements of NADH oxidation rate. Because the integrity of mitochondria was in the range 78–86% the permeability was recalculated for 100% integrity.

as has previously been shown for the closed state of VDAC. However, our observations indicate the opposite result. ATP flux through the channel is not influenced by the overall charge of the channel wall. This conclusion is clearly supported by experiments using VDAC incorporated into planar phospholipid membranes and, additionally, by measurements of metabolite flux across the intact MOM. These observations indicate that general electrostatic interactions between the permeant and the channel do not play a crucial role in the transport of ATP through VDAC. There must be additional interactions that facilitate ATP translocation despite an unfavorable electrostatic environment. The binding site for purine-containing nucleotides is the best candidate for this role.

Interestingly, despite the low primary sequence homology between VDAC isoforms from different species there is remarkable conservation of charged residues at specific positions (41). It would appear that substitution of these with amino acids of similar charge (e.g., lysine for arginine) is not well tolerated. Thus, the distribution of key charged and polar residues may have evolved to provide a better mechanism for metabolite translocation.

Identification of the VDAC binding site requires further investigation. However, our current work clearly

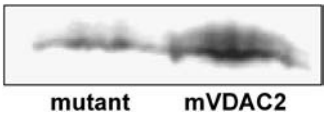

FIGURE 7 SDS-PAGE electrophoresis image of the mutant and mouse VDAC2. The proteins were run in 10% acrylamide gel. The proteins ran at 33 kDa.

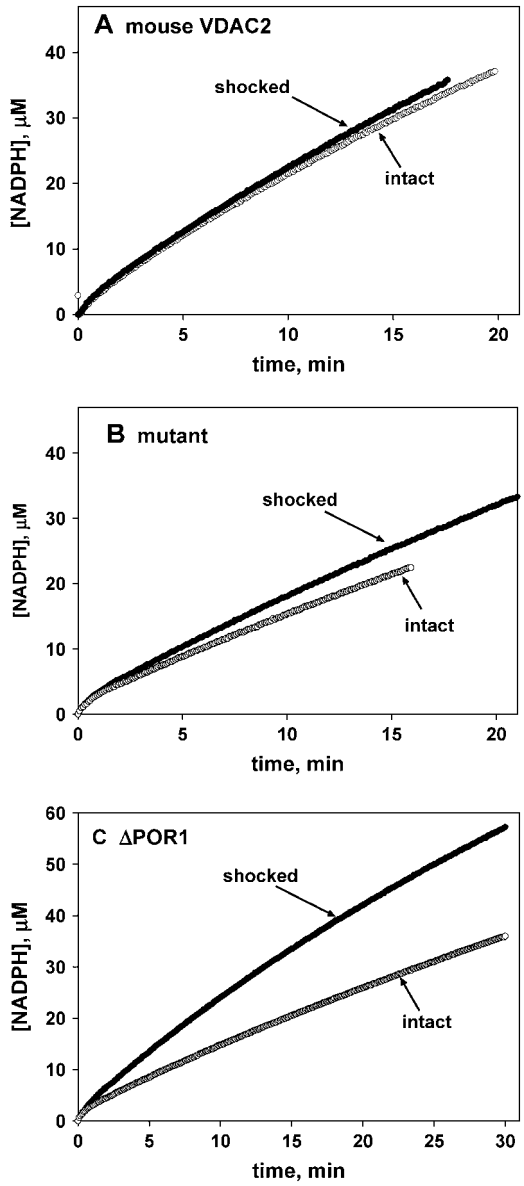

FIGURE 8 Adenylate kinase activity of mitochondria expressing mouse VDAC2 (*A*), the mutant (*B*), or no VDAC (*C*). Reaction was started with addition of 0.25 mM ADP and the NADPH concentration was measured (absorbance at 340 nm). Added enzymes were glucose-6-phosphate dehydrogenase and hexokinase. Concentrations of mitochondrial protein were 280 μg/ml (*A*), 288 μg/ml (*B*), and 250 μg/ml (*C*).

demonstrates that ATP flux through VDAC is not determined by overall charge within the pore but by specific, localized interactive sites where the interaction with VDAC overrides net charge density within the channel. Yet to achieve fast translocation the strength of the overall interaction must be tuned to a precise level. Clearly, large channels are not ''general diffusion pores'' but show a specificity that is dependent on an intimate interaction between the permeant and the channel wall.

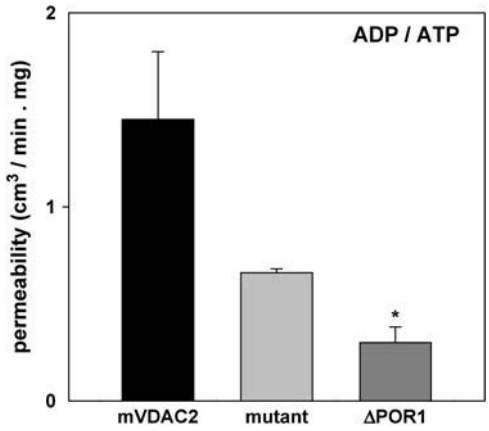

FIGURE 9 A comparison of the average permeability (per milligram protein) of the MOM to ADP/ATP in the presence of mouse VDAC2, the mutant, or in the absence of VDAC (ΔPOR1). The average and the standard deviation were calculated based on the results for different batches of mitochondria (two for each type of mitochondria). The average permeability for each batch was obtained from three independent measurements of NADPH reduction rate. Because the integrity of mitochondria was in the range 78–86% the permeability was recalculated for 100% integrity.

APPENDIX

We estimated ATP flux using the current at zero voltage ($V = 0$) and the permeability ratio (P_{ATP}/P_{Na}). The permeability ratio was determined using the Nernst-Planck flux equation. This theory assumes electrical neutrality in the permeability pathway.

The formulas for the total current and for individual ion fluxes are:

$$I = z_+F\phi_+ + z_-F\phi_- \qquad \text{(Eq.1)}$$

$$\phi_- = -P_-a_-\left(RT\frac{1}{a_-}\frac{da}{dx} + z_-F\frac{dV}{dx}\right) \qquad \text{(Eq.2)}$$

$$\phi_+ = -P_+a_+\left(RT\frac{1}{a_+}\frac{da}{dx} + z_+F\frac{dV}{dx}\right), \qquad \text{(Eq.3)}$$

where ϕ is the flux, P is the permeability, a is the ion activity, and z is the valence.

Using these formulas we obtain the flux of ATP at zero voltage:

$$\phi_{ATP} = \frac{I_{(V=0)}}{|z|F(P_{Na}/P_{ATP} - 1)}, \qquad \text{(Eq.4)}$$

where z is the effective valence of ATP in the solution.

To get the permeability ratio from the measured reversal potential we used an equation from Gincel et al. (42):

$$\sum_i z_i^2 P_i \frac{\{[a]_{cis} - [a]_{trans}B^{z_i}\}}{1 - B^{z_i}} = 0, \qquad \text{(Eq.5)}$$

where a is the ion activity and $B = e^{(F/RT)Vrev}$.

In the case of sodium ATP salt Eq. 5 gives us:

$$\frac{P_{ATP}}{P_{Na}} = \frac{1 - B^z}{z^2(B-1)} \quad \left\{\frac{[Na]_{cis} - [Na]_{trans}B}{[ATP]_{cis} - [ATP]_{trans}B^z}\right\}. \qquad \text{(Eq.6)}$$

The effective valence of ATP (z) was taken from Rostovtseva et al. (17) and is equal to -1.4.

Activity ratios for ATP and Na were calculated using the Nernst equation. For this purpose the values of reversal potential were measured separately in the presence of ideally selective cation and anion membranes.

The final values are: $P_{Na} / P_{ATP} = 17$

$$\phi_{ATP} = 3.3 \times 10^6 \text{ ions/s}.$$

We thank Michael Forte for kindly providing the yeast Δ*POR1* strain.

This work was supported by National Institutes of Health grant R01 NS42319 and the Baylor College of Medicine Child Health Research Center.

REFERENCES

1. Colombini, M. 1979. A candidate for the permeability pathway of the outer mitochondrial membrane. *Nature*. 279:643–645.
2. Mannella, C. A., and M. Colombini. 1984. Evidence that the crystalline arrays in the outer membrane of Neurospora mitochondria are composed of the voltage-dependent channel protein. *Biochim. Biophys. Acta*. 774:206–214.
3. Mannella, C. A., M. Forte, and M. Colombini. 1992. Toward the molecular structure of the mitochondrial channel, VDAC. *J. Bioenerg. Biomembr*. 24:7–19.
4. Lee, A. C., X. Xu, E. Blachly-Dyson, M. Forte, and M. Colombini. 1998. The role of yeast VDAC genes on the permeability of the mitochondrial outer membrane. *J. Membr. Biol*. 161:173–181.
5. Xu, X., W. Decker, M. J. Sampson, W. J. Craigen, and M. Colombini. 1999. Mouse VDAC isoforms expressed in yeast: channel properties and their roles in mitochondrial outer membrane permeability. *J. Membr. Biol*. 170:89–102.
6. Colombini, M. 1980. Structure and mode of action of a voltage dependent anion-selective channel (VDAC) located in the outer mitochondrial membrane. *Ann. N. Y. Acad. Sci*. 341:552–563.
7. Colombini, M. 1987. Regulation of the mitochondrial outer membrane channel, VDAC. *J. Bioenerg. Biomembr*. 19:309–320.
8. Mannella, C. A. 1989. Structure of the mitochondrial outer membrane channel derived from electron microscopy of 2D crystals. *J. Bioenerg. Biomembr*. 21:427–437.
9. Song, J., C. Midson, E. Blachly-Dyson, M. Forte, and M. Colombini. 1998. The topology of VDAC as probed by biotin modification. *J. Biol. Chem*. 273:24406–24413.
10. Abrecht, H., E. Goormaghtigh, J. M. Ruysschaert, and F. Homble. 2000. Structure and orientation of two voltage-dependent anion-selective channel isoforms. An attenuated total reflection Fourier-transform infrared spectroscopy study. *J. Biol. Chem.* 275:40992–40999.
11. Colombini, M. 1989. Voltage gating in the mitochondrial channel, VDAC. *J. Membr. Biol*. 111:103–111.
12. Song, J., C. Midson, E. Blachly-Dyson, M. Forte, and M. Colombini. 1998. The sensor regions of VDAC are translocated from within the membrane to the surface during the gating processes. *Biophys. J*. 74: 2926–2944.
13. Schein, S. J., M. Colombini, and A. Finkelstein. 1976. Reconstitution in planar lipid bilayers of a voltage-dependent anion-selective channel obtained from paramecium mitochondria. *J. Membr. Biol*. 30:99–120.
14. Rostovtseva, T., and M. Colombini. 1997. VDAC channels mediate and gate the flow of ATP: implications for the regulation of mitochondrial function. *Biophys. J*. 72:1954–1962.
15. Rostovtseva, T. K., A. Komarov, S. M. Bezrukov, and M. Colombini. 2002. Dynamics of nucleotides in VDAC channels: structure-specific noise generation. *Biophys. J*. 82:193–205.
16. Rostovtseva, T. K., and S. M. Bezrukov. 1998. ATP transport through a single mitochondrial channel, VDAC, studied by current fluctuation analysis. *Biophys. J*. 74:2365–2373.
17. Rostovtseva, T. K., A. Komarov, S. M. Bezrukov, and M. Colombini. 2002. VDAC channels differentiate between natural metabolites and synthetic molecules. *J. Membr. Biol*. 187:147–156.
18. Blachly-Dyson, E., S. Peng, M. Colombini, and M. Forte. 1990. Selectivity changes in site-directed mutants of the VDAC ion channel: structural implications. *Science*. 247:1233–1236.
19. Sampson, M. J., R. S. Lovell, and W. J. Craigen. 1997. The murine voltage-dependent anion channel gene family. Conserved structure and function. *J. Biol. Chem*. 272:18966–18973.
20. Daum, G., P. C. Bohni, and G. Schatz. 1982. Import of proteins into mitochondria. Cytochrome b2 and cytochrome c peroxidase are located in the intermembrane space of yeast mitochondria. *J. Biol. Chem*. 257: 13028–13033.
21. Clarke, S. 1976. A major polypeptide component of rat liver mitochondria: carbamyl phosphate synthetase. *J. Biol. Chem*. 251: 950–961.
22. Douce, R., J. Bourguignon, R. Brouquisse, and N. Neuburger. 1987. Isolation of plant mitochondria: general principles and criteria of integrity. *Methods Enzymol*. 148:403–412.
23. Ohnishi, T., K. Kawaguchi, and B. Hagihara. 1966. Preparation and some properties of yeast mitochondria. *J. Biol. Chem*. 241:1797–1806.
24. Sotocassa, G. L., B. Kuylenstierna, L. Ernster, and A. Begstrand. 1967. Separation and enzymatic properties of the inner and outer membranes of rat liver mitochondria. *Methods Enzymol*. 10:448–463.
25. Su, S., and P. J. Russell. 1967. Adenylate kinase from baker's yeast (II. Substrate specificity). *Biochim. Biophys. Acta*. 132:370–378.
26. Mannella, C. A. 1982. Structure of the outer mitochondrial membrane: ordered arrays of porelike subunits in outer-membrane fractions from Neurospora crassa mitochondria. *J. Cell Biol*. 94:680–687.
27. Freitag, H., R. Benz, and W. Neupert. 1983. Isolation and properties of the porin of the outer mitochondrial membrane from Neurospora crassa. *Methods Enzymol*. 97:286–294.
28. Montal, M., and P. Mueller. 1972. Formation of bimolecular membranes from lipid monolayers and a study of their electrical properties. *Proc. Natl. Acad. Sci. USA*. 69:3561–3566.
29. Bezrukov, S. M., and I. Vodyanoy. 1993. Probing alamethicin channels with water-soluble polymers. Effect on conductance of channel states. *Biophys. J*. 64:16–25.
30. Laemmli, U. K. 1970. Cleavage of structural proteins during the assembly of the head of Bacteriophage T_4. *Nature (Lond.)*. 227:680–685.
31. Blachly-Dyson, E., E. B. Zambronicz, W. H. Yu, V. Adams, E. R. McCabe, J. Adelman, M. Colombini, and M. Forte. 1993. Cloning and functional expression in yeast of two human isoforms of the outer mitochondrial membrane channel, the voltage-dependent anion channel. *J. Biol. Chem*. 268:1835–1841.
32. Rostovtseva, T. K., and M. Colombini. 1996. ATP flux is controlled by a voltage-gated channel from the mitochondrial outer membrane. *J. Biol. Chem*. 271:28006–28008.
33. Szmelcman, S., and M. Hofnung. 1975. Maltose transport in Escherichia coli K-12: involvement of the bacteriophage lambda receptor. *J. Bacteriol*. 124:112–118.
34. Luckey, M., and H. Nikaido. 1980. Specificity of diffusion channels produced by lambda phage receptor protein of Escherichia coli. *Proc. Natl. Acad. Sci. USA*. 77:167–171.
35. Kullman, L., M. Winterhalter, and S. M. Bezrukov. 2002. Transport of maltodextrins through maltoporin: a single-channel study. *Biophys. J*. 82:803–812.
36. Nestorovich, E. M., C. Danelon, M. Winterhalter, and S. M. Bezrukov. 2002. Designed to penetrate: time-resolved interaction of single antibiotic molecules with bacterial pores. *Proc. Natl. Acad. Sci. USA*. 99:9789–9794.
37. Gellerich, F. N., and W. Kunz. 1987. Cause and consequences of dynamic compartmentation of adenine nucleotides in the mitochondrial intermembrane space in respect to exchange of energy-rich phosphates

between cytosol and mitochondria. *Biomed. Biochim. Acta.* 46:S545–S548.

38. Gellerich, F. N., Z. A. Khuchua, and A. V. Kuznetsov. 1993. Influence of the mitochondrial outer membrane and the binding of creatine kinase to the mitochondrial inner membrane on the compartmentation of adenine nucleotides in the intermembrane space of rat liver mitochondria. *Biochim. Biophys. Acta.* 1140:327–334.
39. Bezrukov, S. M., I. Vodyanoy, R. A. Brutyan, and J. J. Kasianowicz. 1996. Dynamics and free energy of polymers partitioning into a nanoscale pore. *Macromolecules.* 29:8517–8522.
40. Berezhkovskii, A. M., and S. M. Bezrukov. 2005. Optimizing transport of metabolites through large channels: molecular sieves with and without binding. *Biophys. J.* 88:L17–L19.
41. Song, J., and M. Colombini. 1996. Indication of a common folding pattern for VDAC channels from all sources. *J. Bioenerg. Biomembr.* 28:153–161.
42. Gincel, D., H. Zaid, and V. Shoshan-Barmatz. 2001. Calcium binding and translocation by the voltage-dependent anion channel: a possible regulatory mechanism in mitochondrial function. *Biochem. J.* 358:147–155.